



Cite this: *Phys. Chem. Chem. Phys.*,  
2022, **24**, 15973

Received 18th March 2022,  
Accepted 6th June 2022

DOI: 10.1039/d2cp01308h

[rsc.li/pccp](https://rsc.li/pccp)

## Transport signatures of few-atom carbon rings

Carlos Rojas,<sup>a</sup> A. León,<sup>b</sup> M. Pacheco,<sup>b</sup> Leonor Chico<sup>a,c</sup> and P. A. Orellana<sup>\*a</sup>

We study the electronic transport through an all-carbon quantum ring side-coupled to a quantum wire. We employ both first-principles calculations and a tight-binding approach; the latter allows for the derivation of analytical expressions for the conductance and density of states, which facilitates the interpretation of the transport characteristics. Two bond models are employed: either all the hoppings are equal (cumulenic ring) or they have alternating bonds (polyynic ring). Assuming cumulenic bonds, if the number of atoms in the carbon ring is a multiple of four, it produces an antiresonant peak in the conductance at the Fermi level. This effect disappears for the polyynic configuration, *i.e.*, when the hoppings in the carbon rings are alternating. Additionally, a gap opens at the Fermi energy in the polyynic rings, yielding distinct transport signatures for the two bond configurations. Comparison to first-principles calculations shows an excellent agreement on the changes of the conductance due to the carbon ring. We propose such transport measurements as a way to elucidate the character of the bonds in these novel carbon nanostructures.

## 1 Introduction

During the past decades, there has been an increasing interest in the study of molecular electronic devices, dominated by quantum mechanical laws at the single-molecule scale. Within this regime, the discovery of new synthetic carbon allotropes like fullerenes, carbon nanotubes, and graphene opened new avenues for the advancement of electronics.<sup>1–3</sup> Lately, rings of two-coordinate carbon atoms called cyclo[*n*]carbons ( $C_n$ ) have been suggested as an alternative family of molecular carbon allotropes playing an essential role in the formation of fullerenes. Some of them have not been structurally characterized or studied in condensed phases, but recently, the synthesis of the all-carbon molecule  $C_{18}$  from an organic precursor was reported<sup>4</sup>. Regarding cyclocarbons, a controversial and fundamental question concerns whether they are polyynic, that is, with alternating single and triple bonds of different lengths, or cumulenic, with consecutive double bonds.<sup>5–9</sup> Because of this, the electronic and molecular structure of cyclo[*n*]carbons have been topics of theoretical debate. For example, regarding the synthesis of  $C_{18}$ , previous studies of its structure with density functional theory (DFT) and Møller–Plesset perturbation theory predict that the lowest-energy geometry of  $C_{18}$  is cumulenic

(perfect  $D_{18h}$  symmetry),<sup>5,6</sup> whereas Hartree–Fock<sup>10–12</sup> and high-level Monte Carlo and coupled clusters methods suggest that the cyclic polyacetylene configuration with alternating bond lengths ( $D_{9h}$  symmetry) is the ground state.<sup>7,8</sup> Although this dispute has been experimentally settled for  $n = 18$ , which has been shown to be of polyynic nature,<sup>4</sup> other configurations might be possible for  $n \neq 18$ . One means to elucidate the energy spectra of these molecules is by studying their signatures in the electronic transport of a coupled quantum wire. Motivated by the already mentioned characteristics of cyclocarbons, we address a theoretical study of the electronic and transport properties of a carbon ring side-attached to a conducting wire.

Previous works<sup>13–15</sup> indicate that a theory based on the single-electron picture can explain many interesting results in the electronic transport, such as the appearance of antiresonances. Such simplification of the model is also done in order to carry out an analytical treatment. Working in this formalism we show that the system develops an oscillating conductance behavior, with resonances and antiresonances. Besides, a remarkable dependence on the size of the carbon ring was found. In particular, if the number of carbon atoms in the ring is a multiple of four, an antiresonance appears at the Fermi level in the cumulenic configuration. We also compare to first-principles calculations in order to verify the adequateness of our analytical results, finding an excellent agreement between the two approaches.

The article is organized as follows: in Section 2, the geometry of the system is detailed. The formulation for the linear conductance and density of states (DOS) is established in terms of

<sup>a</sup> Departamento de Física, Universidad Técnica Federico Santa María, Casilla 110 V, Valparaíso, Chile. E-mail: [pedro.orellana@usm.cl](mailto:pedro.orellana@usm.cl)

<sup>b</sup> Instituto de Ciencias Básicas, Facultad de Ingeniería, Universidad Diego Portales, Avda. Ejército 441, Santiago, Chile

<sup>c</sup> GISC, Departamento de Física de Materiales, Facultad de Ciencias Físicas, Universidad Complutense de Madrid, 28040 Madrid, Spain

the single-particle Green's functions in order to derive an analytical solution which eases the analysis and interpretation of the results. In Section 3, the relevant physical quantities conductance and DOS are presented, paying special attention to the positions of the antiresonances in the linear conductance spectrum. A comparison to DFT calculations is performed, showing an excellent agreement with the tight-binding model. Finally, the main results are summarized in Section 4.

## 2 Geometry and models

The system under consideration consists of a carbon ring and a quantum wire, the latter is represented by a homogeneous linear chain of carbon atoms; we define  $N$  and  $M$  as the number of atomic sites in the wire and the ring respectively. The ring is connected at an arbitrary location in the wire denoted as  $j$ . The wire also acts as a bridge coupled in series with leads approximated by a continuum of free states, mimicking the presence of large electron reservoirs. The full system is illustrated in Fig. 1.

Within the tight-binding (TB) approximation, the total Hamiltonian of the system is

$$H = H_w + H_r + H_{wr} + H_i. \quad (1)$$

The first term is the Hamiltonian for the wire and is given by

$$H_w = \sum_{i=1}^N \varepsilon_i c_i^\dagger c_i - t \sum_{i=1}^{N-1} (c_{i+1}^\dagger c_i + c_i^\dagger c_{i+1}), \quad (2)$$

where  $c_i^\dagger(c_i)$  is the electron creation (annihilation) operator of an electron at site  $i$  of the wire. The wire onsite energy is assumed to be equal to zero and the hopping energy is set to  $t$ . The second term is the Hamiltonian for the isolated ring and reads

$$H_r = \sum_{p=1}^M \varepsilon_p d_p^\dagger d_p - \sum_{p=1}^{M-1} v_p (d_{p+1}^\dagger d_p + \text{h.c.}) \quad (3)$$

where  $v_p = v_1, v_2$  if  $p$  is odd or even respectively. Here  $d_p^\dagger(d_p)$  is the electron creation (annihilation) operator of an electron, assuming again that the energy for the atomic sites in the ring is zero; and  $v_{1,2}$  are the hopping terms between the atoms in the ring. In order to model the cumulenic geometry of the ring we set  $v_1 = v_2$ , whereas for the polyynic form  $v_1$  and  $v_2$  have

different values. The third term in the Hamiltonian is the coupling between the wire and the ring, given by

$$H_{wr} = -V(c_j^\dagger d_1 + d_1^\dagger c_j), \quad (4)$$

where  $V$  stands for the coupling parameter between site  $j$  in the wire and site 1 of the ring. Finally, the last term in the Hamiltonian represents the interaction with the leads

$$H_i = - \sum_{k_L} V_{k_L}^L (f_{k_L}^\dagger c_1 + c_1^\dagger f_{k_L}) - \sum_{k_R} V_{k_R}^R (f_{k_R}^\dagger c_N + c_N^\dagger f_{k_R}), \quad (5)$$

where  $f_{k_\alpha}^\dagger(f_{k_\alpha})$  is the creation (annihilation) operator of an electron in the continuous state  $k_\alpha$  and the coupling between each lead is given by the terms  $V_\alpha$  where  $\alpha = L, R$ . For the sake of simplicity we set all the onsite energies equal to zero for both the ring and the wire.

We study the electronic transport within the Landauer approach, where the two-terminal conductance  $G$  at zero temperature is proportional to the total transmission for electrons at the Fermi energy  $E_F$ ,

$$G = \frac{2e^2}{h} T(E_F). \quad (6)$$

The total transmission is obtained from the knowledge of the molecular energy levels of each isolated system, making use of the Fisher–Lee relation

$$T = 4\text{Tr}\{\Gamma^L \tilde{G} \Gamma^R \tilde{G}^\dagger\}, \quad (7)$$

where  $\tilde{G}$  is the Green's function matrix for the full problem and  $\Gamma^\alpha = \frac{i}{2}(\Sigma^\alpha - \Sigma^{\alpha\dagger})$  is the spectral matrix density of the  $\alpha = L, R$  lead, which has nonzero elements  $\Gamma_{11}^L$  and  $\Gamma_{NN}^R$  for the system under consideration, since only the first and last atom of the wire are coupled to the leads. Thus, the formula for the conductance simplifies to

$$G = \frac{8e^2}{h} \Gamma_{11}^L \Gamma_{NN}^R |\tilde{G}_{1N}|^2. \quad (8)$$

The matrix element  $\tilde{G}_{1N}$  in the latter expression is obtained from the Dyson equation:

$$\tilde{G}_{1N} = \frac{G_{1N}}{(1 - G_{11}\Sigma^L)(1 - G_{NN}\Sigma^R) - G_{1N}^2\Sigma^L\Sigma^R}, \quad (9)$$

where the Green's functions  $G_{1N}$ ,  $G_{NN}$  and  $G_{11}$  are also obtained from the Dyson recursive formula. For simplicity, the self-energies are chosen  $\Sigma^L = \Sigma^R = -i\Gamma$ , since our concern is to model the effects produced by the ring on the conductance.

Additionally, the density of states of the carbon ring serves as an aid to elucidate the transport properties of the full system:

$$\rho = -\frac{1}{\pi} \text{Im} \left[ \sum_{m=1}^M \tilde{G}_{mm} \right]. \quad (10)$$

DFT calculations were also performed, where the electronic properties of the systems were obtained using the OPENMX

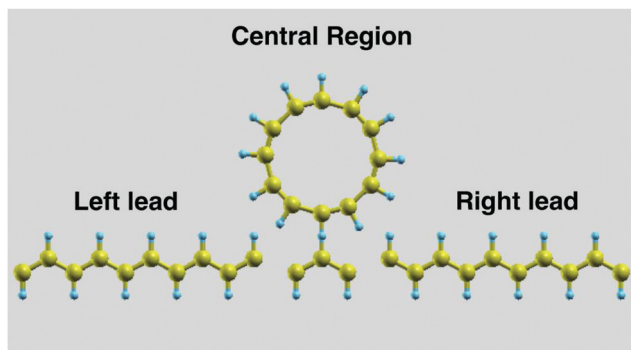


Fig. 1 Schematic representation of the system, where  $N = 3$  and  $M = 12$ .

code,<sup>16</sup> based on localized pseudoatomic orbitals (PAOs)<sup>17</sup> and norm-conserving pseudopotentials.<sup>18</sup> The PAOs of carbon atoms consist of two *s* orbitals and two *p* orbitals. The Perdew–Burke–Ernzerhof (PBE) exchange–correlation functional<sup>19</sup> derived within the GGA is used, with an energy cutoff equal to 150 Ry and a convergence criterion of  $10^{-8}$  Hartree. For calculations of the electronic band structure, 50 *k* points were chosen along each high-symmetry line ( $\Gamma$ –*X* line) in the first Brillouin zone. A  $50 \times 50 \times 1$  Monkhorst–Pack *k*-space mesh is used to discretize the first Brillouin zone. The Gaussian and tetrahedron methods are employed for the DOS calculations.<sup>20</sup> The Fermi energy calculated through the DFT method enters in the tight-binding calculations as a free parameter.

## 3 Results and discussion

### 3.1 Cumulenic geometry

Once we obtain the Green's functions, we can calculate the conductance as a function of the energy levels of the wire and the carbon ring. To begin with, we focus on the study of the isolated wire and ring in order to determine their influence on the system. Fig. 2 shows the conductance and density of states of the system without the ring, *i.e.*, the wire connecting the two electrodes.

The number of resonant peaks exactly matches the number of atomic sites in the wire and their positions reveal its energy spectrum.<sup>21</sup> It should be noted that for *N* odd the wire generates a resonant peak at  $E = 0$ . Therefore, we consider that the 3-site chain is an optimal choice because it has a simple energy spectrum and avoids additional couplings in the first-principles calculations as well as the occurrence of a resonance at the Fermi level.

The cumulenic structure is modeled by setting all the hopping parameters of the ring equal to *t*, *i.e.*, the hopping of the wire. The transmission for different values of the total atomic sites *M* is analyzed, specifically focusing on rings with an even number of atoms. This choice is motivated by the high interest in the recently synthesized  $C_{18}$  molecule<sup>22–27</sup> and also because  $C_n$  molecules are particularly stable when  $n = 4k + 2$

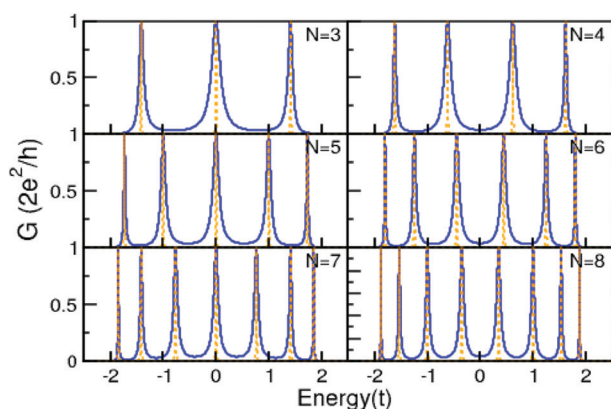


Fig. 2 Conductance (blue) and density of states (orange) of the wire vs. energy for several atomic sizes.

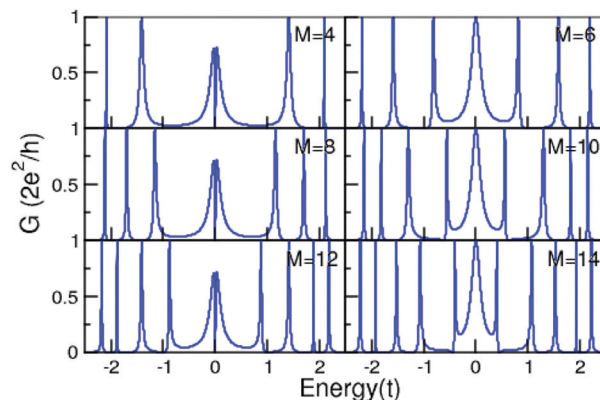


Fig. 3 Conductance vs. energy for several rings in the cumulenic configuration.

(with *k* being an integer),<sup>26,28</sup> as correctly predicted by Pitzer and Clementi in 1959.<sup>29</sup> Fig. 3 displays the transmission for several rings, setting the connection with the ring at the central atom of the wire.

The system exhibits an oscillating pattern of resonances and antiresonances. The antiresonances that appear at the Fermi level for rings with size  $M = 4m$  (with *m* integer) are clearly related to the spectra of the carbon rings, so it is important to compare these features to the energy levels of isolated rings. Their energy spectra are presented in Fig. 4, obtained from the tight-binding model. Indeed, we verify that there is an antiresonance in the conductance of the system for each energy level of the carbon ring. For example, for the  $M = 4$  carbon ring the antiresonance is pinned at the Fermi level, while for  $E = -2t$  and  $E = 2t$  the conductance is exactly zero, but resonant peaks also appear very close to these energies. It is also noticeable for this configuration the energy shift of the conductance resonances due to the chain, which are at the Fermi level and around  $E = \pm 1.5t$ . They are recognizable for  $M = 4$ . However, for  $M = 8$  they are displaced in energy because of the proximity of

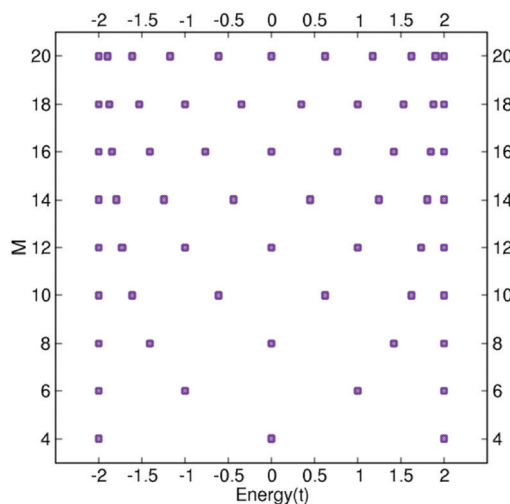


Fig. 4 Energy spectrum of the isolated rings from  $M = 4$  to  $M = 20$  for the cumulenic configuration in the tight-binding model.

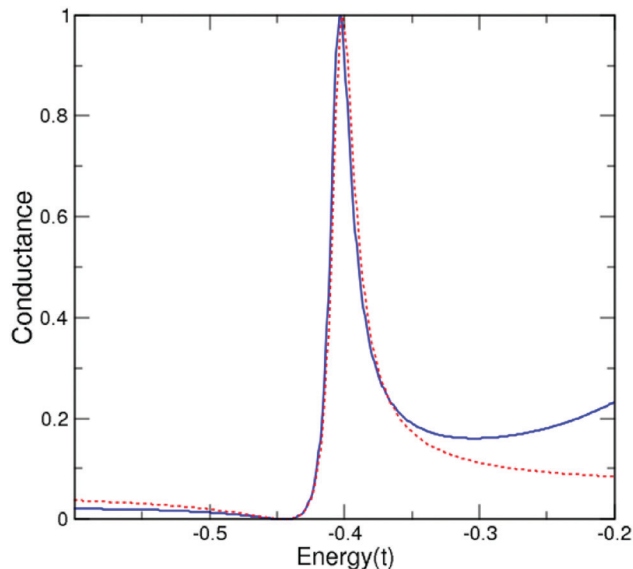


Fig. 5 Conductance of the system with a ring of atomic size  $M = 14$  (blue) and a Fano lineshape (red) with  $q = 4$  and  $\Gamma = 0.02t$ .

the ring and chain states for these energies. Consequently, the hybridization of the states shifts the resonances of the chain towards  $E = \pm t$ .

Both the chain-related resonances and the ring antiresonances can be explained by the Fano effect,<sup>30</sup> where the interference between two scattering amplitudes, one within a continuum of states (the metallic leads) and the second due to an excitation of a discrete state, *i.e.*, those of the carbon ring and chain. The energy dependence of the scattering amplitude is given by the normalized Fano lineshapes

$$F(q; \varepsilon) = \frac{1}{1 + q^2} \frac{(q + \varepsilon)^2}{1 + \varepsilon^2},$$

where  $\varepsilon = 2(E - E_R)/\Gamma$  is the dimensionless reduced energy, which measures the energy relative to the position of the resonance  $E_R$  in units of resonance width  $\Gamma$ , and  $q$  is a dimensionless Fano parameter that determines the form of the Fano lineshapes. For small values of this parameter, ( $q \rightarrow 0$ ) the Fano-Beutler function describes an almost symmetrical drop to zero around the energy of the resonance. It occurs when the discrete system is laterally coupled to the continuum, thus explaining the antiresonance of the ring around its energy levels. In contrast, if a discrete system is embedded in a continuum of states, such as that of the wire, the shape parameter tends to infinity ( $q \rightarrow \infty$ ), and the transmission shows an asymmetrical resonance centered on the discrete energy. Fig. 5 shows a comparison between the conductance profiles for  $M = 14$  and Fano lineshapes.

The characteristic antiresonance profile at the Fermi level occurs for all carbon rings with a number of atomic sites  $M$  multiple of 4. This is due to the structure of energy levels of the rings, which is obtained analytically and is given by

$$\varepsilon_n = -2t \cos\left(\frac{2\pi n}{M}\right), \quad n = 1, 2, \dots, M. \quad (11)$$

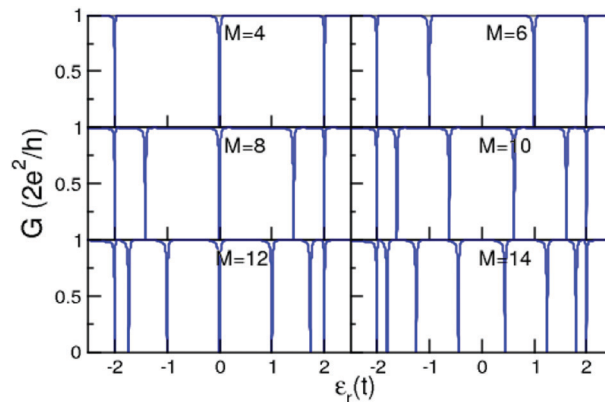


Fig. 6 Conductance vs. onsite energy of the rings for the cumulenlic configuration.

Thus, it is easy to see that there is always an energy level at  $-2t$ . Moreover, if  $M$  is even, there is a state at  $\varepsilon_n = 2t$  ( $n = M/2$ ). Besides, it is straightforward to show that for carbon rings with  $M = 4m$ , where  $m \in \mathbb{N}$ ,  $\varepsilon_n = -2t \cos(n\pi/2m)$ ,  $n = 1, 2, \dots, 4m$ . Then, if  $n/m$  is an odd integer,  $\varepsilon_n$  coincides with the Fermi energy. This happens for  $n = m$  and  $n = 3m$ ; therefore, all carbon rings with  $M = 4m$  will have a doubly degenerate state at the Fermi level, which is reflected as an antiresonance in the conductance for  $E = 0$ . In general, if  $M = pm$ ,

$$\varepsilon_n = -2t \cos\left(\frac{2\pi n}{p m}\right), \quad n = 1, 2, \dots, pm,$$

there is always a degenerate energy  $\varepsilon_p = -2t \cos(2\pi/p)$  for  $n = m$  and  $n = (p - 1)m$ . This antiresonances have been also observed in coupled quantum dot rings.<sup>31</sup> A related system is a side-coupled chain, which presents an even-odd effect in the position of the antiresonances, due to the different energy spectrum of the linear chain.<sup>32</sup> In fact, the position of antiresonances in the conductance is given by the eigenvalues of the side-coupled ring or chain.<sup>31,32</sup>

A gate voltage can be used to move the energy levels of the ring to the Fermi energy. This can be modeled by a variation of the onsite energies of the carbon ring atoms, which produces an antiresonance in the conductance of the system, as represented in Fig. 6, which shows the conductance set at  $E = 0$  as a function of the onsite energy of the atoms in the ring. In this way, the energy spectrum of any ring can be known by analyzing the transport properties of a conductor coupled to the ring. The antiresonances appearing in the conductance of the system are characteristic of the bond configuration and number of atoms of the structure.

We also present a comparison between the results already shown, obtained with the TB model, and DFT calculations. In this way, we can assess the validity of using a simple model to explain transport phenomena in quantum systems. Before presenting the conductance of the whole system, we first consider the subsystems: the conductor, *i.e.*, the carbon chain without the coupled ring, and the isolated ring. Note that the main fitting parameter of the tight-binding model is the

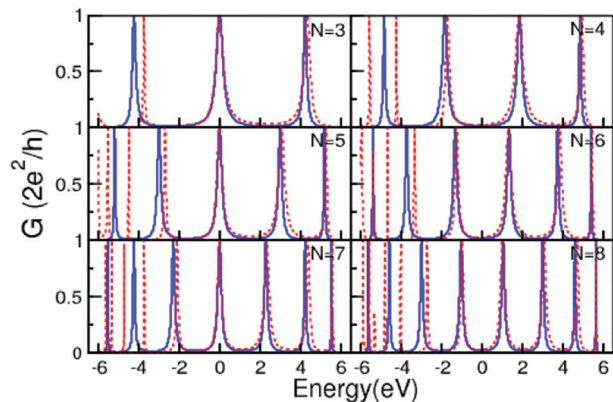


Fig. 7 Comparison between the TB (blue) and the DFT calculations (red) for the conductance of the isolated atomic chain.

hopping energy, which we find to be around  $t = 3$  eV. Fig. 7 shows the conductance of the atomic chain, where the red line represents the DFT calculations, that adjusts very well to the TB model near the Fermi level and for positive values of energy.

Fig. 8 presents the energy spectrum of the isolated carbon rings in an energy range close to the Fermi level. A remarkable similarity between the results of the two models is patent. Obviously, DFT calculations include more orbitals than our TB model; in some cases, we have to shift in energy the DFT results, setting the same Fermi energy in both models in order to make the comparison. For  $M = 4m$  the similarities around the Fermi energy were evident. However, for other carbon rings like  $M = 10$  and  $M = 14$ , an energy shift is necessary. The shift is performed by including a nonzero site energy  $\varepsilon_p$  in the TB approach. This sufficed to adjust the states of all the rings. We note that the value of the energy shift  $\varepsilon_p$  depends on the number of carbon atoms  $M$ .

In addition to this, DFT calculations allows us to obtain the molecular orbitals of the HOMO and LUMO states for a  $M = 12$  ring at the Fermi level, as shown in Fig. 9, which reveals the

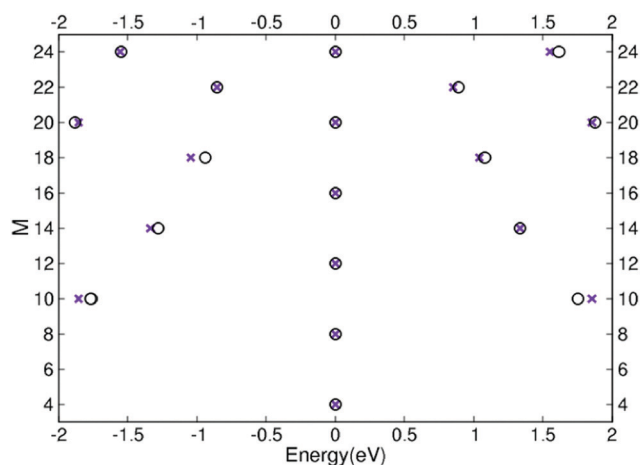


Fig. 8 Comparison between TB model (cross) and DFT calculations (circle) on the energy spectrum of the isolated rings from  $M = 4$  to  $M = 24$  near the Fermi level. A cumulenic configuration is assumed.

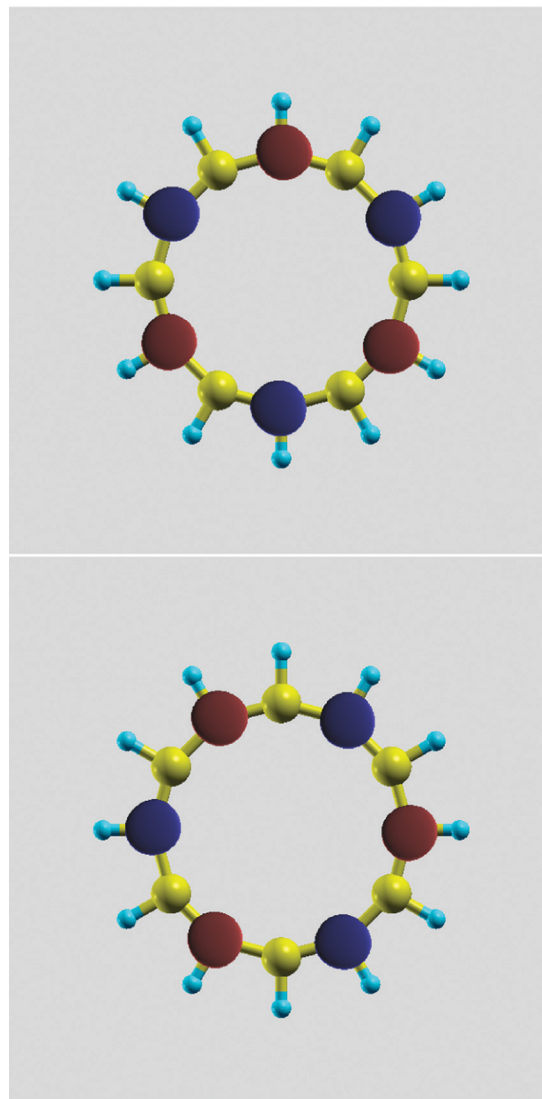


Fig. 9 Molecular orbitals for the HOMO (upper panel) and LUMO (lower panel) states of a ring with  $M = 12$  in the cumulenic configuration at the Fermi level. Colors represent the sign of the eigenfunction: red for positive values and blue for negative values.

nonbonding nature of the states at zero energy. The nodes and the positive/negative signs of the wavefunction can be explained by taking into account that the rings present spatial inversion symmetry.

In particular, for Fig. 9 with  $M = 12$  and for all rings with  $M = 4m$  where  $m \in \mathbb{N}$ , we have a degenerate state at the Fermi level. As discussed previously from eqn (11),  $\varepsilon = 0$  for two values of the wavenumber, namely,  $k = \pi/2$  and  $k = 3\pi/2$ . Although the corresponding eigenfunctions do not have a well-defined parity, we can construct linear combinations of these eigenfunctions which are also parity eigenfunctions. The symmetric and antisymmetric combinations represented by cosine and sine functions explains the sign of the wavefunction in Fig. 9, so that  $\cos(\pi j/2)$  is zero for  $j$  odd, and is equal to  $\pm 1$  for  $j$  even, thus the presence of six nodes, three positive and three negative values for the wavefunction is clearly justified. Also as we can see that

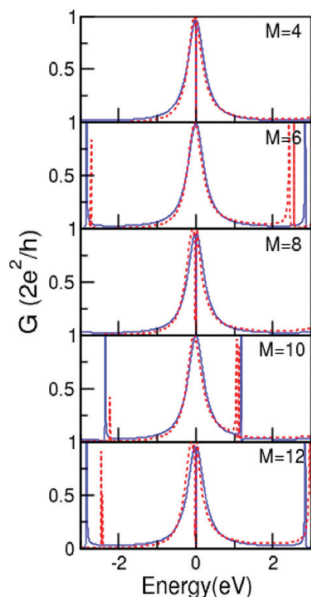


Fig. 10 Comparison between TB (blue) and DFT calculations (red) for the conductance of the whole system. A cumulenic configuration in the ring is assumed.

where there is a node in the HOMO state, the wave function is different from zero in the LUMO state, we can check that by looking at the antisymmetric part of the wavefunction  $\sin(\pi j/2)$ , which is zero for  $j$  even, and equal to  $\pm 1$  for  $j$  odd.

Finally, Fig. 10 displays the comparison between the conductances obtained from the two models around the Fermi level. In this case, this was made so that the blue curve representing the TB model fits the DFT calculations. The most important observation regarding the conductance of the system is the clear antiresonance that appears at the Fermi level for carbon rings with  $M = 4m$  in both models. It is also important to note that for the other rings with  $M \neq 4m$ , the peaks that appear due to the carbon ring are not symmetric, in contradistinction to the TB model. This is best seen by analyzing the conductance for the 10-site ring system and comparing it to Fig. 3.

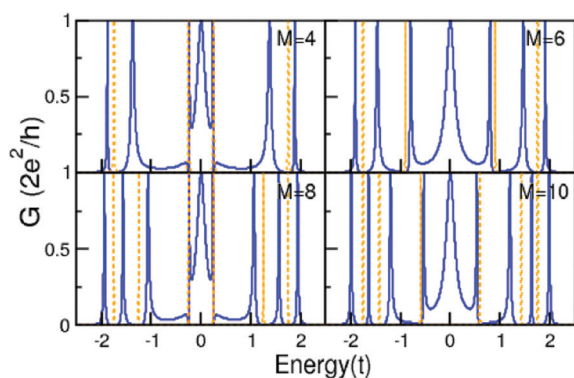


Fig. 11 Conductance vs. energy (blue) and density of states (orange) of the isolated carbon rings for the polyynic geometry.

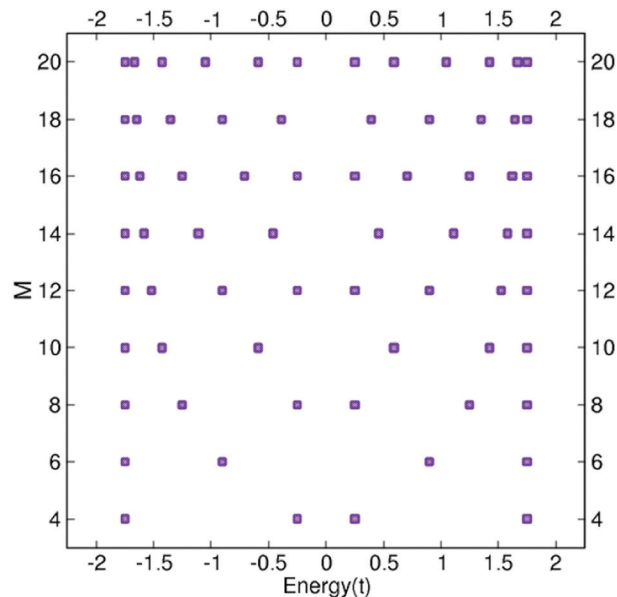


Fig. 12 Energy spectra of the isolated rings from  $M = 4$  to  $M = 20$  for the polyynic configuration in the tight-binding model.

### 3.2 Polyacetylene geometry

For the polyynic cyclic form of the carbon ring, we must consider the difference in the length of the single and triple bonds. These differences in alternating bond lengths represented by the hopping parameter  $\nu$  are considered in the Hamiltonian  $H_r$ , eqn (3). As in the previous section, the energies are given in units of  $t$ , setting  $\nu_1 = t$ , while the other hopping parameter is  $\nu_2 = 0.75t$ . We depict the conductance for rings with these characteristics and the density of states of the isolated carbon rings in Fig. 11.

In the cumulenic configuration, we can observe that the carbon ring generates antiresonances at the positions of its energy levels. The most notable change for the conductances of Section 3.1 is that the antiresonance that occurs at the Fermi level for carbon rings with  $M = 4m$  disappears. This is due to the

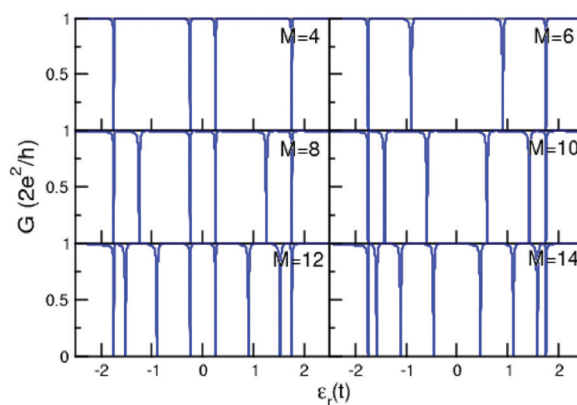


Fig. 13 Conductance vs. onsite energy of the carbon rings in a polyynic configuration.

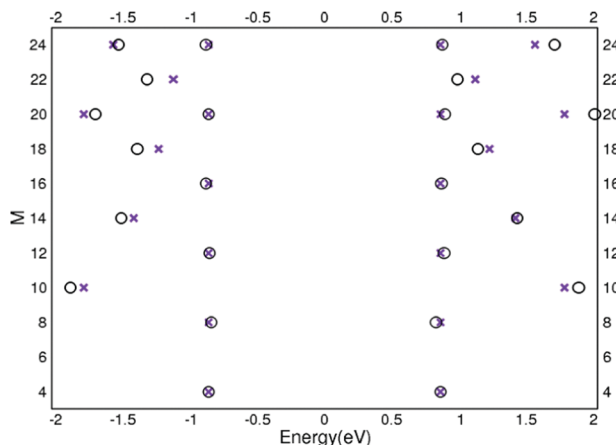


Fig. 14 Comparison between TB model (cross) and DFT calculations (circle) on the energy spectrum of the isolated rings from  $M = 4$  to  $M = 24$  near the Fermi level. A polyynic configuration is assumed.

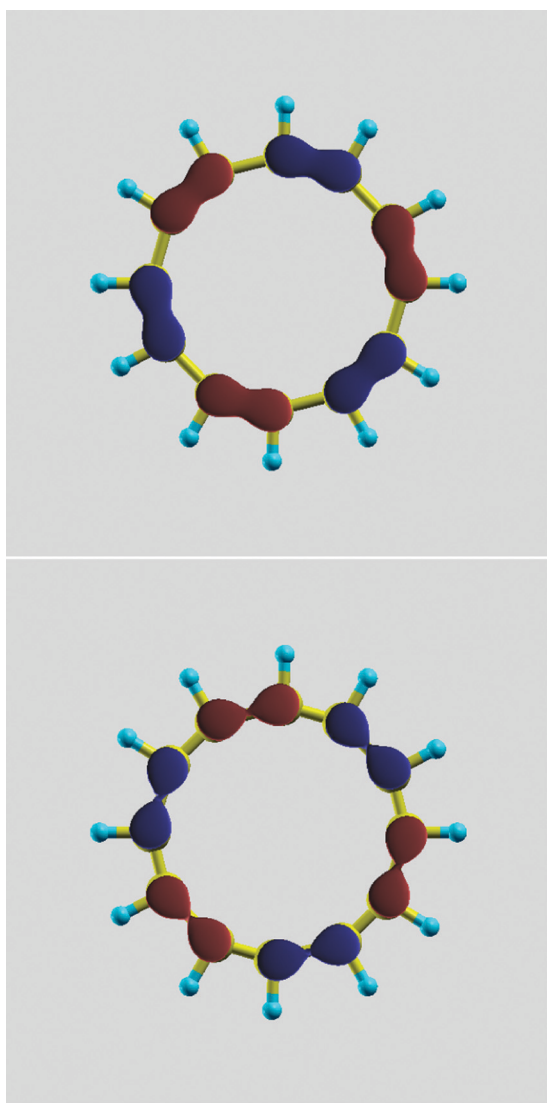


Fig. 15 Molecular orbital for the HOMO (upper panel) and LUMO (lower panel) states of a ring with  $M = 12$  in the polyynic configuration.

change in the hoppings of the rings, which produces a different energy spectrum given by

$$\varepsilon_n = \pm t \sqrt{1 + r^2 + 2r \cos\left(\frac{4\pi n}{M}\right)}, \quad (12)$$

with  $r = v/t$ , the ratio between the hopping in the carbon ring. For carbon ring with  $M = 4m$ , if  $n = m$  then the LUMO and HOMO states are  $\varepsilon_{\text{LUMO}} = t(1 - r)$  and  $\varepsilon_{\text{HOMO}} = -t(1 - r)$ , respectively. This property of the spectrum can be seen in Fig. 12. Since  $M = 2m$ , where  $m \in \mathbb{N}$ , now the possible values for the number  $n$  are  $n = 1, 2, \dots, m$ , all of them give nonzero values for the energy. Therefore, no antiresonance occurs in the Fermi level; for example, for  $M = 4$  the carbon ring has energy levels in  $E = \pm 0.25t$  and  $E = \pm 0.75t$ . It is evident in Fig. 13 that there are antiresonances at those points. We can also see that the energy gap around the Fermi level is the same for all rings with  $M = 4m$ ; this is seen both in the conduction and in the energy spectra of the isolated carbon rings.

Also, Fig. 13 shows the conductance set at the Fermi energy  $E = 0$  as a function of the onsite energy of the atoms in the carbon ring. As we can observe, the spectrum of the carbon ring is reflected in the antiresonances of the conductance. Thus, it proves again that the conductance measurements can be an

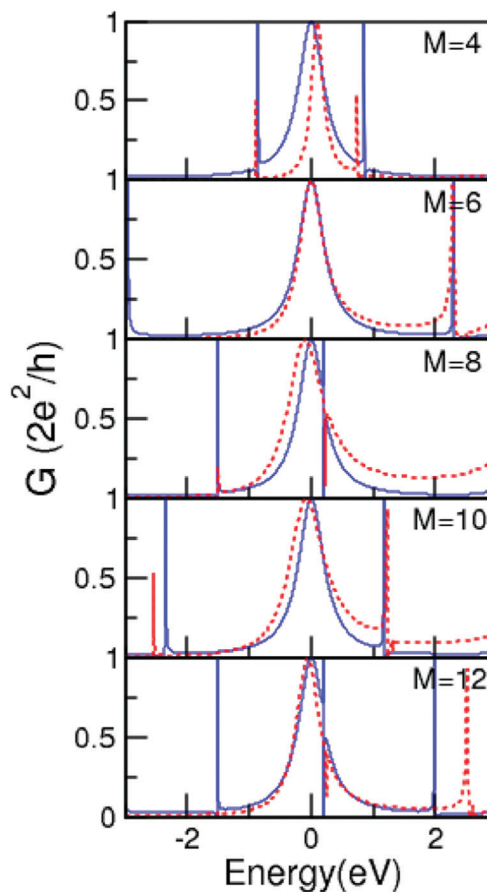


Fig. 16 Comparison between the TB (blue) and DFT calculations (red) for the conductance of the whole system. A polyynic configuration in the ring is assumed.

alternative to assess the carbon ring energy spectrum. DFT calculations were also carried on for this case. Fig. 14 shows the comparison of the energy spectrum of the rings between the two models. As in the case of the cumulenic configuration, the rings with  $M = 4m$  adjusted satisfactorily while the others needed an energy shift to equalize the Fermi levels in both models. Fig. 15 displays the orbital for the HOMO (upper panel) and LUMO (lower panel) states of a isolated ring with  $M = 12$  in the polyynic configuration. As we can see, molecular bonds are formed in this configuration.

This readjustment was also done to compare values of the conductance close to the Fermi level, and the results are shown in Fig. 16. As expected, there are no antiresonances at the Fermi energy ( $E = 0$ ). However, the asymmetry in the positions of the peaks due to the carbon ring in the DFT calculations is more noticeable even for carbon rings with  $M = 4m$ , such as  $M = 8$  and  $M = 12$ , which present an antiresonance very close to  $E = 0$ . Despite this, the energy difference between peaks due the ring is very similar in both models, as commented in the previous cases.

## 4 Conclusions

In this article, we investigate the spectrum and the conductance of a carbon ring coupled to a carbon wire, with two bond ring configurations, cumulenic and polyynic. We find that the system presents a series of resonances and antiresonances due to the coupling of the carbon ring levels to the wire continuum. Resonances due to the chain and the antiresonances of the ring occur in the energy levels of the respective subsystems, both for the cumulenic and polyynic configurations. For the cumulenic case with  $M = 4m$  there is an antiresonance in the conductance at the Fermi energy. This does not happen for the polyynic rings; in fact, they present a gap around the Fermi energy. These changes in the electronic spectra yield distinct transport behaviors. We have verified our TB results against DFT calculations, showing an remarkable agreement, both for the transport and DOS results, in the region of validity of the TB one-orbital model. Therefore, we conclude that transport measurements of a side-connected carbon ring may be a way to elucidate the nature of the bond configuration of the molecule.

## Conflicts of interest

There are no conflicts to declare.

## Acknowledgements

This work has been partially supported by Universidad Santa María Grant USM-DGIIP PI-LI 1925 and 1919 and FONDECYT Grants 1201876 and 1211913, Spanish MCIN and AEI and the European Union under Grant PGC2018-097018-B-I00 (MCIN/AEI/FEDER, UE).

## Notes and references

- 1 K. S. Novoselov, A. K. Geim, S. V. Morozov, D.-E. Jiang, Y. Zhang, S. V. Dubonos, I. V. Grigorieva and A. A. Firsov, *Science*, 2004, **306**, 666–669.
- 2 H. W. Kroto, J. R. Heath, S. C. O'Brien, R. F. Curl and R. E. Smalley, *Nature*, 1985, **318**, 162–163.
- 3 S. Iijima and T. Ichihashi, *Nature*, 1993, **363**, 603–605.
- 4 K. Kaiser, L. M. Scriven, F. Schulz, P. Gawel, L. Gross and H. L. Anderson, *Science*, 2019, **365**, 1299–1301.
- 5 V. Parasuk, J. Almlof and M. W. Feyereisen, *J. Am. Chem. Soc.*, 1991, **113**, 1049–1050.
- 6 C. Neiss, E. Trushin and A. Görling, *ChemPhysChem*, 2014, **15**, 2497–2502.
- 7 T. Torelli and L. Mitás, *Phys. Rev. Lett.*, 2000, **85**, 1702.
- 8 S. Arulmozhiraja and T. Ohno, *J. Chem. Phys.*, 2008, **128**, 114301.
- 9 R. Hoffmann, *Tetrahedron*, 1966, **22**, 521–538.
- 10 F. Diederich, Y. Rubin, C. B. Knobler, R. L. Whetten, K. E. Schriver, K. N. Houk and Y. Li, *Science*, 1989, **245**, 1088–1090.
- 11 G. V. Baryshnikov, R. R. Valiev, A. V. Kuklin, D. Sundholm and H. Ågren, *J. Phys. Chem. Lett.*, 2019, **10**, 6701–6705.
- 12 A. J. Stasyuk, O. A. Stasyuk, M. Solà and A. A. Voityuk, *Chem. Commun.*, 2020, **56**, 352–355.
- 13 K. Bao and Y. Zheng, *Phys. Rev. B: Condens. Matter Mater. Phys.*, 2006, **73**, 045306.
- 14 Z. Y. Mijbil, *Solid State Commun.*, 2019, **287**, 13–18.
- 15 E. Dias and N. Peres, *J. Phys.: Condens. Matter*, 2015, **27**, 145301.
- 16 <http://www.openmx-square.org/>, 2021.
- 17 T. Ozaki and H. Kino, *Phys. Rev. B: Condens. Matter Mater. Phys.*, 2005, **72**, 045121.
- 18 I. Morrison, D. Bylander and L. Kleinman, *Phys. Rev. B: Condens. Matter Mater. Phys.*, 1993, **47**, 6728.
- 19 J. P. Perdew, K. Burke and M. Ernzerhof, *Phys. Rev. Lett.*, 1996, **77**, 3865.
- 20 H. J. Monkhorst and J. D. Pack, *Phys. Rev. B: Solid State*, 1976, **13**, 5188.
- 21 P. Dyachkov, V. Zaluev, E. Y. Kocherga and N. Sadykov, *J. Phys. Chem. C*, 2013, **117**, 16306–16315.
- 22 K. Iyakutti, V. Surya, I. Lakshmi, R. Rajeswarapalanichamy and Y. Kawazoe, *Mater. Sci. Eng., B*, 2021, **263**, 114895.
- 23 H. L. Anderson, C. W. Patrick, L. M. Scriven and S. L. Woltering, *Bull. Chem. Soc. Jpn.*, 2021, **94**, 798–811.
- 24 C. Dai, D. Chen and J. Zhu, *Chem. – Asian J.*, 2020, **15**, 2187–2191.
- 25 Z. Liu, T. Lu and Q. Chen, *Carbon*, 2020, **165**, 461–467.
- 26 G. V. Baryshnikov, R. R. Valiev, R. T. Nasibullin, D. Sundholm, T. Kurten and H. Ågren, *J. Phys. Chem. A*, 2020, **124**, 10849–10855.
- 27 F. Domnguez-Gutiérrez, C. Martnez-Flores, P. Krstic, R. Cabrera-Trujillo and U. von Toussaint, *Radiat. Phys. Chem.*, 2021, **179**, 109166.

- 28 P. W. Fowler, N. Mizoguchi, D. E. Bean and R. W. Havenith, *Chem. – Eur. J.*, 2009, **15**, 6964–6972.
- 29 K. S. Pitzer and E. Clementi, *J. Am. Chem. Soc.*, 1959, **81**, 4477–4485.
- 30 A. E. Miroshnichenko, S. Flach and Y. S. Kivshar, *Rev. Mod. Phys.*, 2010, **82**, 2257–2298.
- 31 P. A. Orellana, M. L. Ladrón de Guevara, M. Pacheco and A. Latgé, *Phys. Rev. B: Condens. Matter Mater. Phys.*, 2003, **68**, 195321.
- 32 P. A. Orellana, F. Domínguez-Adame, I. Gómez and M. L. Ladrón de Guevara, *Phys. Rev. B: Condens. Matter Mater. Phys.*, 2003, **67**, 085321.